



Cite this: *RSC Adv.*, 2021, 11, 34440

Utilizing polymer-conjugate albumin-based ultrafine gas bubbles in combination with ultra-high frequency radiations in drug transportation and delivery†

Thi H. Le,^a An H. T. Phan,^a Khoa C. M. Le,^a Thy D. U. Phan^a and Khoi T. Nguyen ^{*ab}

The application of ultrafine bubbles as drug carriers in drug delivery is still in its developmental stage; it is important to obtain a thorough understanding of the factors affecting the formation and stability of drug carrier matrices. In this study, the polyethylene glycol (PEG)-conjugated human serum albumin (HSA)-based ultrafine bubble simulating the physiological electrolyte concentration in human blood (154 mM) for quercetin delivery was investigated. Optical absorbance measurements, surface tension measurements, and fluorescence laser imaging were also employed to assess the plausibility of polymer-conjugated albumin-stabilized ultrafine bubbles in drug loading and drug release. The incorporation of PEG/HSA into the system illustrated a significant enhancement in the matrix's stability as confirmed by surface tension measurements and drug-loading efficiency achieving approximately 90%. In addition, *in vitro* drug release was performed by the application of high-frequency ultrasound, indicating more than 40% of the loaded quercetin was astonishingly liberated within 5 minutes of exposure.

Received 28th June 2021
Accepted 8th October 2021

DOI: 10.1039/d1ra04983f

rsc.li/rsc-advances

1. Introduction

Advancements in nanotechnology have paved the way to a significant leap in science and engineering. The combination of nanotechnology and medicine has offered improvements in the current drug delivery system with nanocarriers. In a nanocarrier drug delivery system, the medicinal molecules interact with the carrier; after being administered, the drug will leave the carrier slowly and steadily, leading to an increase in the treatment efficiency.¹ Some common nanodrug delivery systems are being researched, including magnetic nanoparticles,^{2–7} micelles,^{8,9} liposomes,¹⁰ dendrimers,¹¹ carbon nanotubes,¹² and nanoemulsions.¹³

Among the mentioned systems, ultrafine bubbles less than 1 micrometer in diameter have ushered in a new appealing realm of drug delivery due to their biocompatibility, biodegradability, adaptability, and nontoxicity in specific biological contexts.^{14–17} These nanoscale air bubbles have been incorporated into various applications in diverse fields owing to their peculiar physicochemical characteristics. While large (sub-millimeters) air bubbles often float quickly to the surface and burst, ultrafine bubbles prefer to remain in the bulk solution for an

extended period of time.¹⁸ This remarkable stability of ultrafine bubbles has accelerated their application in the pharmaceutical industry, especially as drug or gene delivery systems for diagnostic and therapeutic purposes.^{19,20}

Although ultrafine bubbles have been studied for decades, our understanding of them is still in the infant stage; there is still much to exploit. There remain a lot of inquiries regarding the presence and stability of ultrafine bubbles. It has long been assumed that ultrafine bubbles cannot exist for a long time, since the high internal gas pressure of the bubbles induces gas diffusion across the interface resulting in the instantaneous dissolution of such tiny bubbles.²¹ A quasi-stationary model suggests that ultrafine bubbles in pure water dissolve in less than 1 second.²² Another estimation for the lifetime of air bubbles with a radius ranging from 10 to 100 nm gives a duration of 1–100 ns.²³ The collapse of adjacent bubbles in the solution is also considered as another factor responsible for the instability of ultrafine bubbles.²⁴

Various technical approaches have been attempted to elongate the ultrafine bubbles' lifetime to hundreds of seconds or even to over a few months.²⁵ Applying surfactants to the outer shell generates an adsorption monolayer at the interface that helps minimize the interfacial tension and restrict the pressure difference between the inside and the outside of bubbles, hence increasing the bubbles' stability.²⁶ An electrolyte solution is also proposed as a potential alternative to enhance bubbles' lifetime. A low concentration of electrolytes is supposed to extend the lifetime of ultrafine bubbles due to the formation of an ionic

^aSchool of Biotechnology, International University, Vietnam National University, Ho Chi Minh City, Vietnam. Fax: +84(8)3724 4271; Tel: +84(8)3724 4270

^bSchool of Chemical Engineering, The University of Queensland, Brisbane, QLD 4072, Australia. E-mail: nt Khoi@hcmiu.edu.vn

† Electronic supplementary information (ESI) available. See DOI: 10.1039/d1ra04983f



shield, which reduces the dissolution rate of the gas molecules from the gas core to the surrounding solution.²⁷ In our research, we apply electrolytes to inhibit of bubbles coalescence. The electrolyte concentration under investigation imitates the physiological salt concentration in human blood, thus the insights brought by our study will be critical in laying the foundation for the utilization of ultrafine gas bubbles in drug delivery.

Human serum albumin (HSA) is commonly considered for the preparation of stabilized ultrafine bubbles through the formation of a highly elastic layer on the bubbles' surface. This layer can reduce the shrinking rate of gas bubbles and lessen the gas diffusion by minimizing the difference between internal and external bubbles' pressure.²⁸ Moreover, HSA can be applied in the human body due to its biocompatibility, biodegradability, nontoxicity, and non-immunogenicity.²⁹ It has also been proposed as a major matrix component to encapsulate hydrophobic agents through its sub-domain IIA because the hydrophobicity of tryptophan existed in the hydrophobic pocket of this site.^{30,31} In addition to its functionality for transporting various macromolecules in the bloodstream to target organs, it is found that albumin accumulates in solid tumors,^{32,33} making it a potential macromolecular carrier for the site-directed delivery of antitumor drugs. Taking these endowed properties into consideration, HSA is a conceivable therapeutic molecule for drug delivery systems.

Despite its advantages, HSA is structurally sensitive to surrounding conditions and its denaturation may lead to undesirable immunogenic effects.³⁴ Therefore, maintaining the stability of the protein during the process is of chief importance. Among the strategies employed for protein stabilization, chemical modification of protein's surface with a synthetic polymer such as polyethylene glycol (PEG) has been prevalently used to preserve the protein integrity and ameliorate its biocompatibility because of the strong physical adsorption of PEG on the hydrophobic core of HSA.^{35,36} This polymer is non-toxic, non-immunogenic, non-antigenic, highly water-soluble, and is FDA approved.³⁷ Furthermore, the presence of an emulsifying polyethylene glycol coating layer on the bubble shell helps to restrain the interaction with the blood components, thereby reducing the binding of plasma protein to bubbles and enhancing the stability of bubbles in the circulation system.^{38,39} Therefore, in our study, the use of PEG-conjugated HSA to stabilize the protein and ultimately the gas bubbles was investigated.

The sufficient release of therapeutic drugs into target cells or tissues is often a stumbling block in medical applications.⁴⁰ Ultrasound energy has been introduced as an external tool to trigger and increase drug release from nanocarriers, particularly ultrafine bubbles.⁴¹ Recent studies have shown that ultrafine bubbles in combination with high-frequency ultrasound can enhance the pharmaceutical activities of anti-cancer drugs,⁴² and gene therapy.⁴³ Furthermore, acoustic waves have been credited with stimulating cell membrane permeabilization and improving drug absorption by target cells. Therefore, smaller doses of the drug are required compared to the other releasing methods. Pondering on these superior advantages of

ultrasound, this study focuses on the release of drugs by applying high frequency ultrasound to the stabilized ultrafine gas bubble system.

It is imperative to deliberate the interaction behaviour among complex compositions (protein, polymer, drug molecules, and ultrafine bubbles) from the physiochemical perspective. Specifically, the difference between the bulk and the air/water interface is the abundance of air/water interfaces of ultrafine bubbles within the bulk solution. Some researchers have pointed out that the solvation environment strongly affects the physical and chemical properties of a solute.^{44–46} The solvation environment at an air/water interface is extraordinarily dissimilar from that in the bulk solvent because at an interface, a portion of the solute interacts with one medium and the rest is associated with the part of the interface.⁴⁷ Due to this unique situation at the interface, many biological and chemical processes occur at interfaces disparately from those in bulk solvents.⁴⁷ Numerous experiments have been devoted to addressing the similar behaviour of the solute distribution in the bulk and at the interface.⁴⁸ Most of our knowledge about the interface derives from surface tension measurements, which provide an insight into the solute adsorption and distribution at the interface based on the Gibbs adsorption isotherm theory.⁴⁹ Building upon this foundation, our group proposes a novel approach for determining drug loading and releasing efficiency of ultrafine bubbles stabilized by a combination of HSA and PEG using surface tension measurements.

To our knowledge, no such attempts have been made to investigate the utilization of human serum albumin stabilized, polyethylene glycol conjugated ultrafine bubbles for drug delivery. Therefore, we utilized both HSA and PEG for ultrafine bubbles' shell composition to encapsulate drug molecules under physiological conditions. Quercetin was used as a model drug to examine the drug loading and releasing efficacy. In our study, releasing quercetin was assisted by high-frequency acoustic waves to ameliorate drug emancipation. Furthermore, the role of each component constituting the complex was elucidated. We expect that this study might provide preliminary results for the ability of PEG-conjugated HSA stabilized ultrafine bubbles in drug delivery.

2. Materials and methods

2.1 Materials

All chemicals used in this study included sodium chloride (trace metals basis, 99.999% purity, Sigma Aldrich), quercetin (Sigma Aldrich), human serum albumin (Sigma Aldrich), polyethylene glycol 400 (Sigma Aldrich), and ethanol (Sigma Aldrich). Ultrapure Milli-Q unit (Millipore, USA) with a resistivity of 18.2 MW cm was used to prepare all the solutions in the experiments. UV-Vis spectrophotometer (JASCO, model V-730), ultrasonicator (SONICS, Vibra-cell ultrasonic processor model VCX 130 PB, USA), high frequency acoustic wave generator (Portable Ultrasound, 1 MHz), centrifuge (HERMLE LaborTechnik, model Z 306) and CW diode laser source of the violet beam (405 nm) were also used in this study.



2.2 Quercetin-loaded PEG-conjugate albumin ultrafine bubble preparation

500 μM quercetin stock solution was freshly prepared in ethanol. 40 mL of 0.4 mg mL^{-1} human serum albumin (HSA) stock solution was prepared by dissolving 16 mg of HSA in a 154 mM NaCl solution.

Various formulations of quercetin-loaded bubbles were generated in different solutions: (i) physiological salt, (ii) HSA and (iii) HSA conjugated by PEG (Fig. 1). Quercetin and HSA concentrations were maintained at 50 μM and 0.04 mg mL^{-1} , respectively, in all formulations. The ratio of PEG 400: HSA was fixed at 2% (v/v) for HSA stabilization.⁵⁰ These samples were separately sonicated at 20 kHz – 65 W in 20 minutes and the sonicating bath was maintained at room temperature using a water circulation coupled with a water chiller. A sample without bubbles was used as the control in this section.

2.3 Optical absorbance measurement

2.3.1 Experimental method. UV-Visible absorption spectra of quercetin in each solution with the absence and presence of ultrafine bubbles were recorded in the spectral range of 300 to 500 nm using a quartz cuvette of 1 cm path length. The spectra were scanned using a Jasco V-730 spectrophotometer (Jasco International Co. Ltd) with a scanning speed of 55 nm min^{-1} and a data interval of 1 nm. The collected data were analysed using OriginPro 8 software. Quercetin typically has an absorption band in the range of 300–400 nm.⁵¹ Therefore, any change in the absorption spectrum between samples with and without ultrafine bubbles would furnish evidence for the encapsulation of quercetin into gas bubbles and its mutual interaction with other components.⁵²

2.3.2 Drug-loaded bubble detection. Fig. 2 demonstrated the alteration in absorption spectra of samples with and without gas bubbles. The UV-Visible absorption spectrum of quercetin revealed maximum absorption at 368 nm in a sample containing no gas bubbles. Whereas, the spectrum of quercetin-loaded bubbles exhibited four distinct peaks, including a peak still at 368 nm, the others centering at 374 nm, 324 nm, and 423 nm. The decrease of the peak amplitude at 368 nm and the appearance of new peaks at 374 nm, 324 nm, and 423 nm could be contributed by the quercetin molecules adsorbed at the air/water interface of the ultrafine bubbles.

The change in the absorption spectrum of quercetin in the sample with bubbles could be rationalized as the quercetin

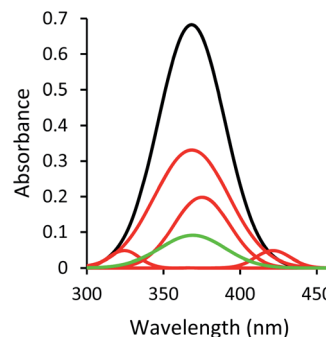


Fig. 2 The change in absorbance spectra of sample without bubbles (—), sample with bubbles (—), and sample with bubbles after centrifugation (—) in PEG/HSA solution. The spectra of sample with bubbles is composed of the absorption spectrum of sample with bubbles.

molecules being attached to the surface of ultrafine bubbles through hydrophobic interaction. The solvated quercetin exhibited its characteristic band at 368 nm, associated with the cinnamoyl group (B- and C-ring), which was highlighted in Fig. S1.†,⁵³ Due to the presence of ultrafine bubbles entailing more hydrophobic surfaces in the solution, the hydrophobic region of quercetin (benzopyran-4-one: A- and C-ring) would have an affinity to the surface of bubbles through hydrophobic interactions. When quercetin molecules were adsorbed at the air/water interface of bubbles, they could not fully interact with solvent molecules as solvated quercetin did, which led to the lower observed peak at 368 nm given by the sample with bubbles compared to the sample without bubbles.

Moreover, the UV-Vis spectrum of quercetin is sensitive to its interaction with the solvent molecules.⁵⁴ The presence of ultrafine bubbles altered this intermolecular interaction *via* hydrophobic forces, engendered the shift in the absorption band of quercetin. In this circumstance, new peaks centered at 374 nm, 324 nm, and 423 nm (Fig. 2) appeared. The regime of quercetin molecules located at the air phase, which is considered as the more hydrophobic condition, could exhibit the shifting in the absorption spectrum compared to solvated quercetin, leading to the observation of a new spectrum in the sample with bubbles.

Briefly, the decrease of the 368 nm peak indicated the lesser amount of fully solvated quercetin; the appearance of the peaks centering at 374 nm, 324 nm, and 423 nm reflected the loading of quercetin into the gas bubbles through hydrophobic interaction with bubbles' surfaces. All of these alterations in the UV-Vis spectrum revealed successful generation of quercetin-loaded ultrafine bubbles.

2.4 Fluorescence laser imaging

The fluorescence laser images radiated by the 405 nm laser beam were obtained by a CCD (Matsushita, 7.5 MP, Venus Engine III). The image analysis extracting the red, green, and blue component channels of the obtained images were analysed by ImageJ software (Version 1.51, the National Institutes of Health, the Laboratory for Optical and Computational Instrumental).

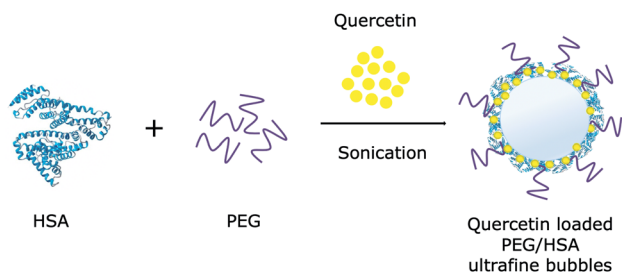


Fig. 1 Schematic representation of quercetin loaded to PEG/HSA stabilized ultrafine bubbles.



2.5 Surface tension measurement

Due to the differences of the solute in the bulk and at the air/water interface, the quercetin adsorption isotherm, which is a plot of surface tension at different quercetin concentrations, was constructed and subsequently used to determine the concentration of quercetin in the bulk solution *via* surface tension values. To construct the quercetin isotherm, a set of surface tension experiments with quercetin concentration in a range of 0–50 μM was conducted.

Surface tension measurements were performed at room temperature using the Wilhelmy plate method. The change in surface tension of samples with and without bubbles along with samples with bubbles after centrifugation was obtained.

2.6 Determination of drug loading efficiency

2.6.1 Experimental method. In order to determine the drug loading efficiency, centrifugation at 6000 rpm for 40 minutes was employed to demolish the bubbles.⁵⁵ The rapid release of the encapsulated drug molecules would cause them to aggregate and ultimately be collected as pellets due to the disturbance of the high centrifuging pressure.⁵⁶ The supernatant after centrifugation was scanned from 300 to 500 nm to detect the free drug concentration. The standard curve of quercetin in each solvated medium was constructed as the function of the peak area (A) at different quercetin concentrations for determining the concentration of quercetin in each circumstance. Therefore, the drug-loading efficiency (EE) could be determined from optical measurements and using the following equation:

$$\text{EE (\%)} = \frac{[\text{quercetin}]_{\text{total}} - [\text{quercetin}]_{\text{free}}}{[\text{quercetin}]_{\text{total}}} \times 100\%$$

$$= \frac{A_{368(\text{total})} - A_{368(\text{free})}}{A_{368(\text{total})}} \times 100\%$$

where, $A_{368(\text{total})}$ is the peak area of the solvated quercetin that was originally introduced to the sample before the bubble generation and $A_{368(\text{free})}$ is the peak area of the free quercetin in the supernatant.

Besides, the drug loading efficacy was also determined by measuring the surface tension of samples with and without bubbles. In conjunction with the plot of surface tension at different concentrations of quercetin, the drug-loaded efficiency (EE) was evaluated using the following equation:

$$\text{EE (\%)} = \frac{[\text{quercetin}]_{\text{total}} - [\text{quercetin}]_{\text{free}}}{[\text{quercetin}]_{\text{total}}} \times 100\%$$

in which, $[\text{quercetin}]_{\text{total}}$ is the initial amount of quercetin introduced to the sample before bubble generation and $[\text{quercetin}]_{\text{free}}$ is the concentration of free quercetin in collected supernatant that was not loaded onto the bubbles; both $[\text{quercetin}]_{\text{total}}$ and $[\text{quercetin}]_{\text{free}}$ were determined by using the corresponding surface tension and the constructed quercetin isotherm (Fig. 3).

2.6.2 Quercetin loading efficiency determination. Samples with bubbles after centrifugation exhibited a single peak centering at 368 nm (Fig. 2). This could be the contribution of free solvated quercetin molecules that did not adsorb at the

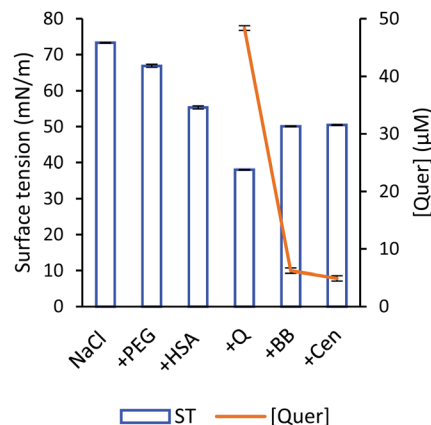


Fig. 3 The change in surface tension in turn PEG (+PEG), HSA (+HSA), quercetin addition (+Q), bubble presence (+BB), and after centrifugation (+Cen) with corresponding quercetin concentration in the bulk at different conditions (initial addition, + BB, and + Cen).

bubbles' interface. Meanwhile, ultrafine bubbles with loaded quercetin were ruptured and released quercetin molecules in aggregated form and later were collected as a pellet by centrifugation.⁵⁷ A slight reduction in the absorption spectrum of the sample without bubbles after centrifugation was also obtained due to the instability of quercetin (Fig. S2†); however, it was not as substantial as in the presence of gas bubbles. Taking these considerations, it was computed that approximately ~86% of the drug was loaded into bubbles obtained from optical measurements.

The Wilhelmy plate measurements revealed that the addition of HSA, PEG, and quercetin were responsible for the decrease in surface tension (Fig. 3). This observation is consistent with the fact that a liquid interface is more easily accessible by the presence of these molecules (HSA, PEG, quercetin), which reduce the value of surface tension.⁵⁷ It is generally acknowledged that if the surface tension of the solution is lower than that of the pure solvent, there is an enhancement of solutes' concentration in the liquid interface, suggesting that these molecules are surface-active in aqueous solutions.⁴⁹ Indeed, these molecules were inclined to be located at the interface due to its amphiphilic behaviour presented by its chemical structure and a drop in surface tension value. By pointing the hydrophobic regimes into the gas phase, these molecules gained more favourable molecular interactions and reduced the surface free energy, prompting to reduce surface tension.⁵⁸

When ultrafine bubbles were generated in the solution, an increase in surface tension was observed (Fig. 3). The quercetin-PEG/HSA complex could adsorb onto the air/water interface of gas bubbles through hydrophobic–hydrophobic interaction. Once attached to ultrafine bubbles, the complex would be retained in the bulk solution, which prevented its effect on the liquid interface. Concurrently, there will still be some free quercetin molecules that are bound to neither HSA nor bubbles and, apparently, these free molecules are mainly responsible for decreasing the surface tension. The amount of free quercetin



was markedly small compared to the amount of loaded quercetin, hence a slight decrease in surface tension was observed.

The similarity of surface tension of the sample with bubbles before and after centrifugation could be explained by the free quercetin at the liquid interface. After centrifugation, these molecules were still solvated in the solution and were ascribed to the descent of surface tension, whereas the loaded quercetin was precipitated due to the collapse of bubbles. The number of free quercetin molecules in both samples with bubbles before and after centrifugation was unchanged, thus the resemblance in surface tension of these samples was attained.

The surface tension measurement results indicated that approximately ~90% amount of quercetin was loaded into PEG/HSA stabilized bubbles. It was in good agreement with UV-Vis measurements that the quantified amount of quercetin loaded into the bubbles formed in the PEG/HSA solution was around 86%. It is rational to observe a slight difference between values obtained from two approaches, given that the dichotomy of solute at the interface and in the bulk solution.

2.7 Control of drug released *in vitro* and determination of releasing efficiency

Drug release has been typically studied by equilibrium dialysis experiments to facilitate the separation of released drugs against the drug/bubbles systems.^{59–61} Unfortunately, in this study, dialysis experiments would not be feasible due to the effect of ultrafine bubbles on the permeability of interested species across the porous membrane. Therefore, the high-frequency acoustic wave (HFA) was chosen to study drug release from the quercetin-loaded ultrafine bubbles due to its bubbles' destruction ability.⁶² Under the influence of HFA, the quercetin/bubbles matrices underwent continuing expansion and compression, resulting in their destruction by either outward diffusion of the gas during the compression phase or by complete fragmentation of the complex's shell and the gas core.^{63–65} When the complex vanished, quercetin molecules would be liberated off in form of pellets, thus the collected sample after release could be used to evaluate drug release efficiency. In this study, a drug release experiment was conducted at room temperature, with the succour of HFA at 1 MHz with the output intensity of 1.6 W cm⁻², 8% duty cycle for 5 minutes. The HFA probe was always placed directly in contact with the glass cell containing 10 mL of the sample *via* coupling gel.

It is worth noting that the released drug and drug/bubble systems critically affect the accuracy of optical instruments. UV-Vis spectra were influenced by the absorption and scattering of the ultrafine bubbles presented in the solution, which is of relevance to Mie scattering theory.⁶⁶ The appearance and disappearance of these submicron bubbles could influence the optical radiation adsorption and change the amount of light reaching the detector leading to an alteration in absorbance and a misinterpretation in the calculation.⁶⁷ In addition, the sample-filtering process prior to the UV-Vis measurement would severely interfere with the gas bubble system being studied. Therefore, UV-Vis measurement might not be adequate for accurate estimation of the drug concentration in the

presence of these species. The amount of drug released from the bubbles could be quantified through the surface tension value of the sample with bubbles after release. The drug release efficiency (RE) was assessed using the equation:

$$\begin{aligned} \text{RE (\%)} &= \frac{[\text{quercetin}]_{\text{released}}}{[\text{quercetin}]_{\text{loaded}}} \times 100\% \\ &= \frac{[\text{quercetin}]_{\text{after HFA}} - [\text{quercetin}]_{\text{before HFA}}}{[\text{quercetin}]_{\text{total}} - [\text{quercetin}]_{\text{before HFA}}} \times 100\% \end{aligned}$$

where, $[\text{quercetin}]_{\text{after HFA}}$ is the total amount of quercetin in the bulk after HFA application, consisting of both the released and the unloaded amount of quercetin, while $[\text{quercetin}]_{\text{before HFA}}$ is composed of the unloaded quercetin in the bulk before HFA application. The $[\text{quercetin}]_{\text{before HFA}}$ and $[\text{quercetin}]_{\text{after HFA}}$ were deduced from the surface tension of the sample before and after HFA application combined with the quercetin adsorption isotherm (Fig. S3†).

3. Results and discussion

3.1 The role of human serum albumin

In the gas bubble-rich media, drug molecules could exist simultaneously in several conformations: (i) fully solvated by the ethanol molecules (Fig. 4a), (ii) partially associated with the gaseous phase of the gas bubbles (Fig. 4b). It is desirable to distinguish the drug molecules in the above conformations. In this drug loading experiment, quercetin was not only solvated *via* hydrogen bonds, but also loaded to bubbles through hydrophobic interaction, the latter of which engendered the change in UV-Vis spectrum of the sample after bubble generation.

The HSA concentration used in this study was chosen to be slightly below the adsorption saturation of HSA at the air/water interface, which was inferred from the HSA isotherm (Fig. S4†). From this isotherm, HSA adsorption started to saturate beyond 0.05 mg mL⁻¹. As the surface was saturated by HSA, the unadsorbed HSA molecules could stay in the bulk solution, limiting the drug loading capacity.⁶⁸ Based on this consideration, 0.04 mg mL⁻¹ HSA solution was chosen for the formulation design of quercetin-loaded ultrafine bubbles.

Physiological salt solution prolonged the bubbles' lifetime due to the inhibition of bubbles' coalescence.⁶⁹ Therefore, HSA in physiological salt solution was believed to further stabilize the

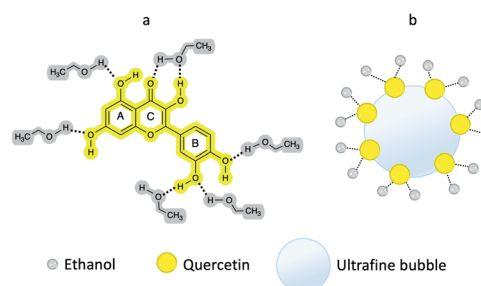


Fig. 4 Schematic representation of different quercetin conformations (a) fully solvated and (b) partially resided at the air/water interface.



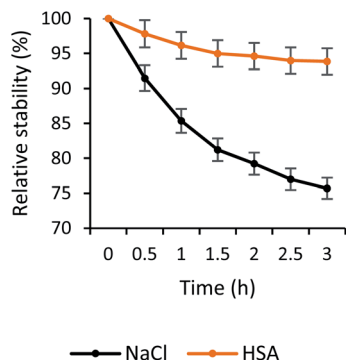


Fig. 5 Stability of quercetin-loaded bubbles in physiological salt and HSA solution within 3 hours.

gas bubbles. Indeed, incorporating HSA into the ultrafine bubbles' shell was equitable for the increase of quercetin-bubbles complex's stability. The quercetin loaded in the ultrafine bubbles in NaCl solution was decomposed roughly 25% within 3 hours, whereas approximately 5% decrease was observed in the case of encapsulated quercetin in HSA-stabilized bubbles (Fig. 5). This indicated that the quercetin-bubbles complex was apparently protected by the HSA addition. Once HSA was presented in the solution, the interaction of quercetin and HSA occurred between the hydrophobic region of quercetin and the hydrophobic part of the HSA cavity.⁷⁰ The A- and C-ring of quercetin would have a tendency to bind to the hydrophobic region of HSA and the B-ring pointed toward the interface of IIB and IIIA domains of HSA,⁵³ consequently, encapsulated and preserved by HSA.

When ultrafine bubbles were introduced to the solution, the HSA-wrapped quercetin complexes were attached to the surface of the bubbles through hydrophobic-hydrophobic interactions. As the attachment between bubble and quercetin/HSA complexes was established, the quercetin molecules could be partially located at the air/water interface or completely associated with HSA (Fig. 6). These quercetin molecules were located at the air/water interface of bubbles, thus they did not interact with solvent molecules as much as those in the sample without bubbles.

Therefore, with HSA, the change in the absorption spectrum was observed to be similar to the case without HSA (Fig. S5†). The reduction of peak amplitude in the bubble solution was contributed by the adsorption of quercetin molecules partially encapsulated to HSA and located at the bubbles' interface. The observed spectrum's shifting was also explained due to the formation of the hydrogen bond between the chromophoric groups of quercetin and auxochromic group of HSA molecules ($-\text{OH}$, $-\text{NH}_2$, $-\text{SH}$, $-\text{OR}$, or $-\text{SR}$).^{71,72} Once the sample with bubbles was centrifuged, the obtained peak at 368 nm could be the contribution of the free solvated quercetin that did not bind to HSA.

In addition, the fluorescence images (illuminated by the 405 nm laser) of samples with/without bubbles and samples with bubbles after centrifugation in different solvated solutions (physiological salt and HSA solution) were obtained as visual detection for the possibility of ultrafine bubbles in the loaded drug (Fig. S6†). As a result, the images revealed a clear change from dark green (sample without bubbles) to violet-red (sample

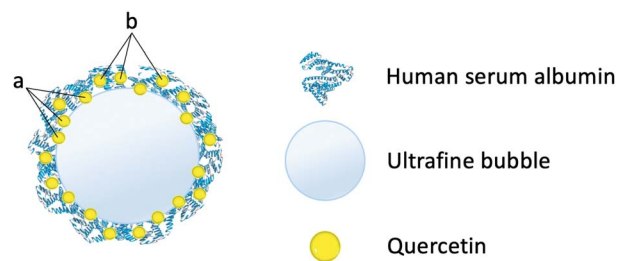


Fig. 6 Schematic representation of quercetin conformation in HSA solution (a) partially associated with HSA and (b) completely attached at HSA binding site.

with bubbles), suggesting the formation of the quercetin-loaded ultrafine bubbles. This was in conformity with the fluorescence emission spectra of quercetin when forming a complex with the neutral molecule, at which an emission peak at around 600 nm was observed.⁷³ Accordingly, the violet-red of the sample with bubbles under exposure of the 405 nm laser could be explained by the contribution of the quercetin either resided at the air/water interface of bubbles or attached at the binding site of albumin. Furthermore, the observed green colour in the image of samples with bubbles after centrifugation was given by free solvated quercetin, showing the bubbles' annihilabilities during centrifugation. According to these observations, HSA hampered the process of quercetin degradation by encapsulating quercetin molecules in its binding sites through hydrophobic interactions. This also furnished evidence for quercetin being indirectly loaded to the ultrafine bubbles as the HSA-quercetin complexes attached onto the bubbles.

3.2 The role of polyethylene glycol

The addition of PEG to the solution aimed to preclude HSA from denaturation caused by the heat formation from the encapsulation process.⁵⁰ In this study, we investigated the relative influence of PEG/HSA stabilized ultrafine bubbles on quercetin delivery. Our results indicated that the stability of encapsulated quercetin in the PEG/HSA-bubbles complex did not decrease substantially within 3 hours as compared to that of quercetin in the HSA-bubbles complex (Fig. 7). That is to say, PEG did not participate in the stabilization of quercetin. It was demonstrated

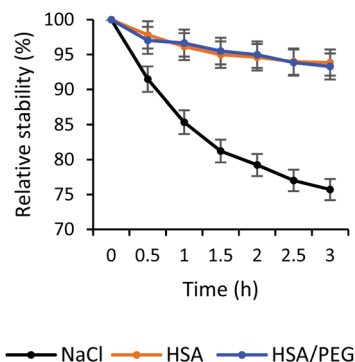


Fig. 7 Stability of quercetin-loaded bubbles in physiological salt, HSA, and PEG/HSA solution within 3 hours.



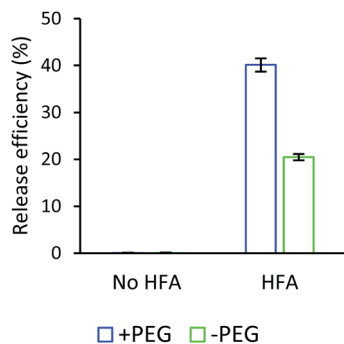


Fig. 8 Release profiles after 5 minutes of HFA exposure in cases of with and without PEG addition.

by the comparability in the spectrum of the sample with PEG/HSA-bubbles (Fig. 2) and the spectrum of the sample with bubbles in the HSA solution (Fig. S5†). The congruence of the change in fluorescence laser images between samples with and without PEG was also observed, demonstrating the presence of drug-bubbles complex in the solution (Fig. S6†).

Interestingly, PEG was considered to accelerate drug liberation in our study. Based on the quercetin isotherm and the change in surface tension before and after release (Fig. S3†), in the instance without PEG, only around 20% of quercetin was liberated in 5 minutes of HFA exposure (Fig. 8). However, in the PEG/HSA-bubbles complex, a good release efficiency was obtained (Fig. 8). The results indicated that more than 40% of quercetin was released from PEG/HSA stabilized bubbles upon identical HFA exposure time. Indeed, the incorporation of PEG into the HSA layer increased the hydrophilicity of the matrix (*i.e.*, promotes the solvent-complex interaction).^{74,75} Under the mechanical impact of HFA, the quercetin liberation was meant to occur much easier than without PEG. Therefore, conjugating PEG to HSA could be considered appropriate for the dual effect of the matrix: (i) improve the ultrafine gas bubble stability and (ii) facilitate the controlled release of drug molecules upon HFA exposure.

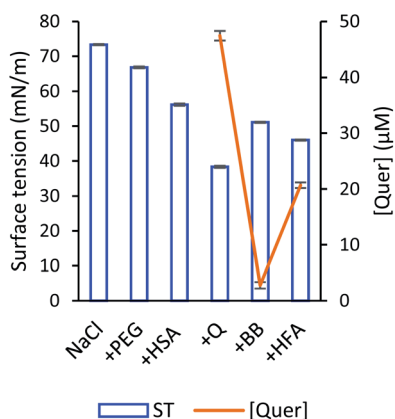


Fig. 9 The change in the surface tension in turns PEG (+PEG), HSA (+HSA), quercetin addition (+Q), bubble presence (+BB), and after released by HFA (+HFA) with corresponding quercetin concentration in the bulk at different conditions (initial addition, +BB, and +HFA) in PEG/HSA solution.

3.3 The role of high-frequency acoustic sound

Ultrafine bubbles are sensitive to the frequency of the acoustic wave,⁷⁶ therefore we executed a control experiment to measure the light scattering of the solution with bubbles before and after acoustic wave application. A small light scattering intensity increase (5.1%) was observed, which indicated the stability of the bubbles system upon our specific ultrasonic excitation.

Fig. 9 demonstrates the change of surface tension with corresponding quercetin concentration of the sample before (+BB) and after HFA application (+HFA). Under the effect of HFA, quercetin molecules being loaded into ultrafine bubbles were released when the ultrafine bubbles started to respond to high-frequency acoustic wave. These continuing contractions and expansions of the gas bubbles shook the loaded quercetin molecules off the bubbles. The newly-released quercetin molecules would then join the solvent system to be solvated. Evidently, the fluorescence imaging excited by the 405 nm laser also demonstrated drug liberation upon the application of HFA (the inset of Fig. S7†). A slight decrease in the red component was recorded in the sample with bubbles after the release as compared with that before the release (Fig. S7†). It is worth mentioning that during HFA exposure, a portion of the gas bubbles might burst and cause some damage to the vessel wall.⁷⁷ However, our control experiment demonstrated that our acoustic excitation did not trigger massive bubble bursting that could cause mechanical damage to the vessel walls.

4. Conclusion

In this study, the plausibility of employing stabilized ultrafine gas bubbles as carriers for drug delivery was investigated. A rational stabilization approach was developed using HSA and PEG 400 as bubble and protein stabilizer agents, respectively. The results confirmed the stabilization of drug-bubbles complex with a protein and polymer for achieving high drug-loading capacity, of which approximately 90% of quercetin was loaded. Furthermore, the crucial role of PEG in releasing the drug was corroborated, in which more than 40% of the loaded quercetin was remarkably released off the ultrafine gas bubbles upon a 5 minutes exposure to high-frequency acoustic sound.

Author contributions

T. L (investigation, methodology, writing-OD, formal analysis, data curation) A. P (investigation, data curation, validation, writing-R and E). K. L (investigation, validation, writing-R and E). T. P (investigation, writing-R and E). K. N (conceptualization, data curation, funding acquisition, methodology, supervision, resources, writing-R and E).

Conflicts of interest

There are no conflicts to declare.



Acknowledgements

This research is funded by Vietnam National Foundation for Science and Technology Development (NAFOSTED) under grant number 106.02.2018.315.

References

- 1 A.-Y. Cai, Y.-J. Zhu and C. Qi, *Adv. Mater. Interfaces*, 2020, **7**, 2000819.
- 2 D. N. Price, L. R. Stromberg, N. K. Kunda and P. Muttill, *Mol. Pharm.*, 2017, **14**, 4741–4750.
- 3 V. Sagar, S. Pilakka-Kanthikeel, V. S. Atluri, H. Ding, A. Y. Arias, R. D. Jayant, A. Kaushik and M. Nair, *J. Biomed. Nanotechnol.*, 2015, **11**, 1722–1733.
- 4 B. S. Ungureanu, C. M. Teodorescu and A. Săftoiu, *J. Gastrointest. Liver Dis.*, 2016, **25**, 375–383.
- 5 M. M. Fathy, H. M. Fahmy, A. M. M. Balah, F. F. Mohamed and W. M. Elshemey, *Life Sci.*, 2019, **234**, 116787.
- 6 F.-H. Chen, L.-M. Zhang, Q.-T. Chen, Y. Zhang and Z.-J. Zhang, *Chem. Commun.*, 2010, **46**, 8633–8635.
- 7 Y. Li, N. Wang, X. Huang, F. Li, T. P. Davis, R. Qiao and D. Ling, *ACS Appl. Bio Mater.*, 2020, **3**, 121–142.
- 8 K. Xiao, J. Luo, W. L. Fowler, Y. Li, J. S. Lee, L. Xing, R. H. Cheng, L. Wang and K. S. Lam, *Biomaterials*, 2009, **30**, 6006–6016.
- 9 A. N. Lukyanov and V. P. Torchilin, *Adv. Drug Delivery Rev.*, 2004, **56**, 1273–1289.
- 10 C. Spuch and C. Navarro, *J. Drug Delivery*, 2011, **2011**, 469679.
- 11 A. S. Chauhan, *Molecules*, 2018, **23**, 938.
- 12 J. Ferluga, U. Kishore and R. B. Sim, *Mol. Immunol.*, 2014, **59**, 188–193.
- 13 M. Kumar, R. S. Bishnoi, A. K. Shukla and C. P. Jain, *Prev. Nutr. Food Sci.*, 2019, **24**, 225–234.
- 14 C. Su, X. Ren, F. Nie, T. Li, W. Lv, H. Li and Y. Zhang, *RSC Adv.*, 2021, **11**, 12915–12928.
- 15 A. Jafari Sojahrood, A. C. de Leon, R. Lee, M. Cooley, E. C. Abenojar, M. C. Kolios and A. A. Exner, *ACS Nano*, 2021, **15**, 4901–4915.
- 16 A. Wijaya, A. Maruf, W. Wu and G. Wang, *Biomater. Sci.*, 2020, **8**, 4920–4939.
- 17 F. Eklund, M. Alheshibri and J. Swenson, *Curr. Opin. Colloid Interface Sci.*, 2021, **53**, 101427.
- 18 A. J. Jadhav and M. Barigou, *Langmuir*, 2020, **36**, 1699–1708.
- 19 Y. Wang, X. Li, Y. Zhou, P. Huang and Y. Xu, *Int. J. Pharm.*, 2010, **384**, 148–153.
- 20 B. E. Oeffinger and M. A. Wheatley, *Ultrasonics*, 2004, **42**, 343–347.
- 21 T. Vehmas and L. Makkonen, *ACS Omega*, 2021, **6**, 8021–8027.
- 22 M. Plesset and S. Sadhal, *Appl. Sci. Res.*, 1982, **38**, 133–141.
- 23 S. Ljunggren and J. Eriksson, *Colloids Surf., A*, 1997, **130**, 151–155.
- 24 M. Jamialahmadi and H. Müller-Steinhagen, *Chem. Eng. J.*, 1992, **50**, 47–56.
- 25 E. Dressaire, R. Bee, D. C. Bell, A. Lips and H. A. Stone, *Science*, 2008, **320**, 1198.
- 26 J. J. Kwan and M. A. Borden, *Adv. Colloid Interface Sci.*, 2012, **183–184**, 82–99.
- 27 J. R. T. Seddon, D. Lohse, W. A. Ducker and V. S. J. Craig, *ChemPhysChem*, 2012, **13**, 2179–2187.
- 28 S. Mahalingam, M. B. Meinders and M. Edirisinghe, *Langmuir*, 2014, **30**, 6694–6703.
- 29 F. Kratz, T. Roth, I. Fichiner, P. Schumacher, H. H. Fiebig and C. Unger, *J. Drug Targeting*, 2000, **8**, 305–318.
- 30 C. Dufour and O. Dangles, *Biochim. Biophys. Acta*, 2005, **1721**, 164–173.
- 31 O. J. Rolinski, A. Martin and D. J. Birch, *J. Biomed. Opt.*, 2007, **12**, 034013.
- 32 Y. Matsumura and H. Maeda, *Cancer Res.*, 1986, **46**, 6387–6392.
- 33 Y. Takakura, T. Fujita, M. Hashida and H. Sezaki, *AAPS J.*, 1990, **7**, 339–346.
- 34 M. J. Farrell, R. J. Reaume and A. K. Pradhan, *Sci. Rep.*, 2017, **7**, 2604.
- 35 O. Annunziata, N. Asherie, A. Lomakin, J. Pande, O. Ogun and G. B. Benedek, *Proc. Natl. Acad. Sci. U. S. A.*, 2002, **99**, 14165–14170.
- 36 S. Rawat, C. Raman Suri and D. K. Sahoo, *Biochem. Biophys. Res. Commun.*, 2010, **392**, 561–566.
- 37 F. M. Veronese and G. Pasut, *Drug Discovery Today*, 2005, **10**, 1451–1458.
- 38 D. D. Lasic, F. J. Martin, A. Gabizon, S. K. Huang and D. Papahadjopoulos, *Biochim. Biophys. Acta*, 1991, **1070**, 187–192.
- 39 M. Ogris, S. Brunner, S. Schüller, R. Kircheis and E. Wagner, *Gene Ther.*, 1999, **6**, 595–605.
- 40 L. B. Feril, Jr. and K. Tachibana, *Int. J. Hyperthermia*, 2012, **28**, 282–289.
- 41 S. Mitragotri, *Nat. Rev. Drug Discovery*, 2005, **4**, 255–260.
- 42 A. Prabhakar and R. Banerjee, *ACS Omega*, 2019, **4**, 15567–15580.
- 43 H. Kida, K. Nishimura, K. Ogawa, A. Watanabe, L. B. Feril, Y. Irie, H. Endo, S. Kawakami and K. Tachibana, *Front. Psychopharmacol.*, 2020, **11**, 363.
- 44 M. F. J. Mabeoone, A. R. A. Palmans and E. W. Meijer, *J. Am. Chem. Soc.*, 2020, **142**, 19781–19798.
- 45 R. Cabot and C. A. Hunter, *Chem. Soc. Rev.*, 2012, **41**, 3485–3492.
- 46 M. D. Driver and C. A. Hunter, *Phys. Chem. Chem. Phys.*, 2020, **22**, 11967–11975.
- 47 S. K. Mondal, S. Yamaguchi and T. Tahara, *J. Phys. Chem. C*, 2011, **115**, 3083–3089.
- 48 A. Kundu, H. Watanabe, S. Yamaguchi and T. Tahara, *J. Phys. Chem. C*, 2013, **117**, 8887–8891.
- 49 T.-M. Chang, in *Physical Chemistry of Gas-Liquid Interfaces*, ed. J. A. Faust and J. E. House, Elsevier, 2018, pp. 1–40, DOI: 10.1016/B978-0-12-813641-6.00001-7.
- 50 N. Samanta, D. D. Mahanta, S. Hazra, G. S. Kumar and R. K. Mitra, *Biochimie*, 2014, **104**, 81–89.
- 51 T. J. Mabry, K. R. Markham and M. B. Thomas, in *The Systematic Identification of Flavonoids*, ed. T. J. Mabry, K. R.

- Markham and M. B. Thomas, Springer Berlin Heidelberg, Berlin, Heidelberg, 1970, pp. 41–164, DOI: 10.1007/978-3-642-88458-0_5.
- 52 F. Zsila, Z. Bikádi and M. Simonyi, *Biochem. Pharmacol.*, 2003, **65**, 447–456.
 - 53 Y. Ni, X. Zhang and S. Kokot, *Spectrochim. Acta, Part A*, 2009, **71**, 1865–1872.
 - 54 M. Buchweitz, P. A. Kroon, G. T. Rich and P. J. Wilde, *Food Chem.*, 2016, **211**, 356–364.
 - 55 M. A. Wheatley, F. Forsberg, N. Dube, M. Patel and B. E. Oeffinger, *Ultrasound Med. Biol.*, 2006, **32**, 83–93.
 - 56 S. A. Abouelmagd, B. Sun, A. C. Chang, Y. J. Ku and Y. Yeo, *Mol. Pharm.*, 2015, **12**, 997–1003.
 - 57 C. R. A. Mouzouvi, A. Umerska, A. K. Bigot and P. Saulnier, *PLoS One*, 2017, **12**, e0179211.
 - 58 R. L. Martin, *Anal. Chem.*, 1963, **35**, 116–117.
 - 59 R. X. Zhang, P. Cai, T. Zhang, K. Chen, J. Li, J. Cheng, K. S. Pang, H. A. Adissu, A. M. Rauth and X. Y. Wu, *Nanomedicine*, 2016, **12**, 1279–1290.
 - 60 S. Modi and B. D. Anderson, *Mol. Pharm.*, 2013, **10**, 3076–3089.
 - 61 J. Shen and D. J. Burgess, *Drug Delivery Transl. Res.*, 2013, **3**, 409–415.
 - 62 K. Yasuda, H. Matsushima and Y. Asakura, *Chem. Eng. Sci.*, 2019, **195**, 455–461.
 - 63 J. E. Chomas, P. Dayton, J. Allen, K. Morgan and K. W. Ferrara, *IEEE Trans. Sonics Ultrason.*, 2001, **48**, 232–248.
 - 64 A. Bouakaz, M. Versluis and N. de Jong, *Ultrasound Med Biol.*, 2005, **31**, 391–399.
 - 65 D. J. May, J. S. Allen and K. W. Ferrara, *IEEE Trans. Sonics Ultrason.*, 2002, **49**, 1400–1410.
 - 66 P. Chýlek and J. Zhan, *Appl. Opt.*, 1990, **29**, 3984.
 - 67 B. Van Eerdenbrugh, D. E. Alonzo and L. S. Taylor, *Pharm. Res.*, 2011, **28**, 1643–1652.
 - 68 P. Maffre, S. Brandholt, K. Nienhaus, L. Shang, W. J. Parak and G. U. Nienhaus, *Beilstein J. Nanotechnol.*, 2014, **5**, 2036–2047.
 - 69 V. S. J. Craig, B. W. Ninham and R. M. Pashley, *Nature*, 1993, **364**, 317–319.
 - 70 R. Fang, H. Jing, Z. Chai, G. Zhao, S. Stoll, F. Ren, F. Liu and X. Leng, *J. Nanobiotechnol.*, 2011, **9**, 19.
 - 71 A. P. Schenning, V. H. J. P. Jonkheijm, Z. Chen, F. Würthner and E. W. Meijer, *J. Am. Chem. Soc.*, 2002, **124**, 10252–10253.
 - 72 T. W. Bell and N. M. Hext, *Chem. Soc. Rev.*, 2004, **33**, 589–598.
 - 73 J. C. Alva-Ensastegui, M. Palomar-Pardavé, M. Romero-Romo and M. T. Ramírez-Silva, *RSC Adv.*, 2018, **8**, 10980–10986.
 - 74 L. Moradkhannejhad, M. Abdouss, N. Nikfarjam, M. H. Shahriari and V. Heidary, *J. Drug Delivery Sci. Technol.*, 2020, **56**, 101554.
 - 75 P. Ouyang, Y.-q. Kang, G.-f. Yin, Z.-b. Huang, Y.-d. Yao and X.-m. Liao, *Front. Mater. Sci.*, 2009, **3**, 15–24.
 - 76 S. Tanaka, H. Kobayashi, S. Ohuchi, K. Terasaka and S. Fujioka, *Ultrason. Sonochem.*, 2021, **71**, 105366.
 - 77 H. Chen, A. A. Brayman, M. R. Bailey and T. J. Matula, *Urol. Res.*, 2010, **38**, 321–326.

